Applied Catalysis B: Environment and Energy 355 (2024) 124136

Contents lists available at ScienceDirect

Applied Catalysis B: Environment and Energy

journal homepage: www.elsevier.com/locate/apcatb

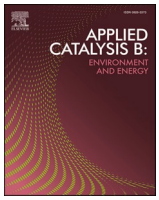

Trap-n-zap: Electrocatalytic degradation of perfluorooctanoic acid (PFOA) with UiO-66 modified boron nitride electrodes at environmentally relevant concentrations

Sheng Yin [a,d], Juan Francisco López [a,d], Christian Sandoval-Pauker [a,d], Jonathan J. Calvillo Solís [a,d], Sarah Glass [b,d], Ahsan Habib [a], Wen-Yee Lee [a], Michael S. Wong [b,c,d], Pedro J.J. Alvarez [b,c,d], Dino Villagrán [a,d,*]

[a] Department of Chemistry and Biochemistry, The University of Texas at El Paso, El Paso, TX 79968, USA
[b] Department of Civil and Environmental Engineering, Rice University, Houston, TX 77005, USA
[c] Department of Chemical and Biomolecular Engineering, Rice University, Houston, TX 77005, USA
[d] Nanosystems Engineering Research Center for Nanotechnology-Enabled Water Treatment (NEWT), USA

ARTICLE INFO

Keywords:
PFOA oxidation
PFAS
Electrocatalysis
Composite catalyst

ABSTRACT

Poly- and per-fluoroalkyl substances (PFAS) are synthetic chemicals of increasing global concern due to their toxicity and environmental persistence. Hexagonal boron nitride (h-BN) is an electrochemically active semiconductor that generates a hydrophobic electron-hole with a high affinity for the fluorinated tail of perfluorooctanoic acid (PFOA), which enhances surface interactions in aqueous solutions. We demonstrate that h-BN electrocatalytically oxidizes PFOA to shorter chains. The degradation is enhanced by modifying the h-BN surface with an adsorbent, UiO-66 (UiO-66@BN), that facilitates proximal adsorption to catalytic sites (trap-and-zap). At the environmentally relevant concentration of 100 μg/L, electrochemical trap-and-zap removes 99.5% of PFOA with 70% defluorination in 3 h at a pH 4.5. Computational results show that PFOA requires an overpotential of 1.87 V *vs.* SCE, which is close to the experimental overpotential. The electrical energy per order (EE/O) of UiO-66@BN is 6.1 kWh/m^3, indicating that it is a competitive material for PFOA electrochemical remediation.

1. Introduction

Poly- and per-fluoroalkyl substances (PFAS) are a large group of industrially relevant, synthetic chemicals used in various applications, such as firefighting, waxes, food packaging, and paints. Their chemical structure is characterized by strong C–F bonds, making them remarkably stable under various physical and chemical conditions [1,2]. The persistent nature of PFAS has led to concerns about their adverse effects on the environment and public health. Perfluorooctanoic acid (PFOA), one of the most common PFAS, has been found in water, soil, plants, animals, and even human bodies [1,2]. Environmental PFOA concentrations have been reported to reach up to 7 mg/L in aqueous conditions [3,4] and 50 mg/kg in soil [5,6]. Chronic PFOA exposure can be linked to many adverse health effects, including high cholesterol, thyroid disease, testicular cancer, kidney cancer, ulcerative colitis, and pregnancy-induced hypertension [7–10]. Due to these concerns, stringent governmental regulations regarding PFOA levels in the environment have been implemented in the USA., China, Europe, and other regions [11,12].

Several water treatment technologies have been employed to remove PFOA from various water matrices, such as adsorption, membrane filtration via reverse osmosis, high-pressure/high-temperature decomposition, and redox-driven processes, such as photochemical [13], electrochemical [14,15], mechanochemical [14], thermal [16], or advanced oxidation/reduction [13,14]. Adsorption and membrane filtration processes remove PFAS without eliminating their liability by transferring the PFAS to another medium that requires additional treatment, time, and energy to eliminate or minimize their toxicity. Thus, technologies that directly destroy PFAS, such as photochemical and electrochemical approaches, are receiving increasing attention [2,14].

Electrochemical methods in water treatment allow for the stable and

* Corresponding author at: Department of Chemistry and Biochemistry, The University of Texas at El Paso, El Paso, TX 79968, USA.
E-mail address: dino@utep.edu (D. Villagrán).

https://doi.org/10.1016/j.apcatb.2024.124136
Received 26 February 2024; Received in revised form 18 April 2024; Accepted 26 April 2024
Available online 29 April 2024

efficient removal of pollutants while having tunable control of direct/indirect oxidation or reduction [17–19]. Electrochemical methods can degrade PFAS to shorter chain or polyfluorinated byproducts, ideally resulting in mineralization (i.e., conversion to F^- and CO_2) [18,20]. The most common electrodes for PFAS electrochemical oxidation are based on boron-doped diamond (BDD) [21], Magneli phase titanium oxide (Ti_4O_7) [22,23], tin dioxide (SnO_2) [24,25], and lead dioxide (PbO_2) [26]. These electrode materials are stable at high current and potential and can generate a significant amount of reactive oxygen species (e.g., •OH radicals), which enhances the hydroxylation and eventual mineralization of PFAS degradation products [24,27,28]. Graphene sponge electrodes [29] and nano-ZnO coated Ti electrodes [30] also show great potential for PFAS degradation. However, all of the reported electrodes show several limitations. PbO_2 and SnO_2 electrodes can release toxic Pb^{2+} or Sn^{2+} ions into aqueous matrices, generating a form of secondary pollution. [31,32] BDD electrodes are limited by high capital costs, making their large-scale application unfeasible. [18,33] Many electrochemical PFAS degradation studies report degradation rates that correspond to PFAS concentrations orders of magnitude higher than those found in the environment. [18] This high concentration may increase the efficacy of the electrode under these conditions, so it is important to perform laboratory tests with environmentally relevant levels for reliable and representative performance assessments. [18] Therefore, efficient, stable, and economically feasible electrodes for PFAS electrochemical oxidation are needed to provide alternative solutions when facing the challenges of PFAS contamination.

Hexagonal boron nitride (h-BN) is a cost-effective, widely available, and scalable semiconductor that can catalyze the photooxidation of PFOA. As a photocatalyst, h-BN is four times more effective for PFOA degradation than the common photocatalyst P25-TiO_2. Its efficacy is partly due to its hydrophobic electron hole, which minimizes the scavenging of its oxidation capacity by the more abundant water molecules [34]. However, photocatalysis has intrinsic limitations. For instance, poor energy efficiency and self-shadowing limit its widespread application. [35] This motivated us to explore the application of h-BN in electrochemical systems, which offers the potential for band gap tunability for its catalytic activity. [36] At low PFOA concentrations, such as those found in environmental conditions, maximizing the PFOA concentration near the electrode surface is important to improve the efficiency of the catalytic degradation. While h-BN has a hydrophobic surface (6−25 m^2/g) [37,38] that is beneficial for PFOA adsorption, it can be further enhanced by the addition of UiO-66, a water-stable zirconium-based metal-organic framework (MOF) with an even larger hydrophobic surface (>1000 m^2/g), to trap PFOA. UiO-66 has been previously reported as an efficient PFOA adsorbent [39–41] and as the basis of an electrochemical sensor. [42] In this work, we functionalized the h-BN surface with UiO-66 (UiO-66@BN) to pre-adsorb and concentrate (trap) PFOA on the electrocatalytic sites of h-BN anodes (zap). We measured the electrochemical activity of UiO-66@BN electrodes at environmentally relevant PFOA concentrations (10–100 μg/L) to validate their oxidation efficiency. We studied the electrochemical behavior of PFOA and its response to changes in initial PFOA concentration, pH, and the presence of various common ions. The mechanism of PFOA oxidation was studied by experimental (gas chromatography-mass spectrometry, GC-MS; cyclic and square wave voltammetry; and electrochemical impedance spectroscopy, EIS) and computational methods (density functional theory (DFT) simulations). This study introduces a novel, sustainable, and reusable method for PFOA treatment using a trap-and-zap approach. By combining experimental studies with computational simulations, insights have been provided into the underlying electrochemical degradation mechanisms and provide the basis for the implementation of h-BN-based electrodes as a viable electrochemical method for PFOA treatment.

2. Materials and methods

2.1. Syntheses

All reagents purchased from commercially available sources were used as received. Boron nitride (BN) and zirconium chloride ($ZrCl_4$) were purchased from Alfa Aesar. N,N-dimethylformamide (C_3H_7NO, DMF), and terephthalic acid ($C_8H_6O_4$, H_2BDC) were purchased from TCI Chemicals. Formic acid (HCOOH) was purchased from Fisher Scientific. Deionized (DI) water from the Milli-Q ultrapure water purification system (Millipore Co.) was used in this study. The synthesis of UiO-66 ($Zr_6O_4(OH)_4(HBDC)_{12}$) followed a published procedure [43].

2.1.1. Synthesis of composite UiO-66@BN (B-4)

0.124 g of h-BN was dispersed in 50 mL of DMF and sonicated for 2 h to prepare a ca. 0.1 M suspension. To this suspension, 1.165 g of $ZrCl_4$ and 0.736 g of BDC (molar ratio of UiO-66:h-BN = 1:1, other molar ratios were calculated accordingly) were added, along with 5.0 mL formic acid. This suspension was then sonicated for 30 min. The mixture was placed in an oven and heated to 80 °C for 12 h and then at 100 °C for 24 h (Eq. 1). After cooling the mixture to room temperature, the product was filtered and washed with DMF (3 times). The solid was suspended in 30.0 mL acetone overnight to remove DMF, rinsed with acetone again (3 times), and dried under vacuum overnight. According to the different ratios of h-BN and UiO-66, (UiO-66:h-BN), the materials are marked as B-1(0.1:1), B-2 (0.2:1), B-3 (0.5:1), B-4 (1:1), B-5 (2:1), and B-6 (10:1).

$$6Zr^{4+} + 8H_2O + 12BDC^{2-} \rightarrow Zr_6O_4(OH)_4(HBDC)_{12} \quad (1)$$

2.1.2. Preparation of electrode

5 mg of h-BN (or composite B-1, B-2, B-3, B-4, B-5, and B-6, accordingly) and 2.5 mg carbon black were mixed in a 3.0 mL scintillation vial. Then 1.0 mL of isopropanol and 4.5 μL Nafion were added. The suspension was sonicated for 15 min to obtain a homogenous dispersion (ink). 50.0 μL ink was carefully drop-coated onto a 1.0 × 0.5 cm^2 carbon paper via a micropipette. The carbon paper was left to dry at room temperature for 1 h. The stability of the components of the electrodes was measured independently before the electrochemical experiments. The F^- concentration after 3 h of electrochemical oxidation in 0.1 M Na_2SO_4 was lower than 10.0 μg/L (Figure S1), which indicates that Nafion does not interfere with the measurements.

2.2. Characterization

The synthesized materials were characterized through FT-IR, p-XRD, and SEM to investigate their optical properties, bond formation, crystallinity, and morphology. BET was performed to investigate the porosity and surface area. Fourier transform infrared (FT-IR) spectra were obtained from an Agilent Cary 630 FT-IR spectrometer. X-ray diffraction (XRD) patterns were measured on a PAN-analytical Empyrean system using Cu-Ka radiation (λ = 1.5418 Å) equipped with a PIXcel [3D] detector. Scanning electron microscope (SEM) was performed on a Hitachi S-4800 instrument. The N_2 adsorption isotherms were obtained using a Micromeritics ASAP-2020 adsorption analyzer at 77 K.

2.3. PFOA electrochemical oxidation

All electrochemical measurements were performed in a single cell with a three electrode electrochemical setup using a CHI760E potentiostat (Figure S2). All prepared electrodes were evaluated by cyclic voltammetry (Table S1) and square wave voltammetry (Table S2). The carbon paper coated with UiO-66@BN was used as the working electrode, Pt wire was used as the counter electrode, and the saturated calomel electrode (SCE, CHI-150) was used as the reference electrode. Cyclic and square wave voltammograms, CV and SWV, respectively,

were measured in 0.1 M Na_2SO_4 solution in the presence and absence of PFOA. N_2 gas was injected to purge oxygen from the solution before the evaluation. Electrochemical impedance spectra (EIS) of the UiO-66@BN electrodes were measured in 0.1 M Na_2SO_4 solution with 100 μg/L PFOA at a voltage amplitude of 5 mV and a frequency range from 10^{-1} to 10^6 Hz. Initial PFOA concentrations of 100 mg/L PFOA were used to facilitate analyses and advance mechanistic understanding. Concentrations ranging from 10 to 100 μg/L were used to validate the performance of the electrocatalytic materials under environmentally relevant conditions.

2.4. Batch experiments

All electrochemical degradation experiments were performed in a single cell with a three-electrode electrochemical setup using a CHI760E potentiostat. The spacing between the reference and the working electrodes was 0.5 cm. The distance between the working and the counter was 1.8 cm. Bulk electrolysis at 1.8 – 2.5 V *vs.* SCE (Table S3) was performed for 3 h 10 mL of a 0.1 M Na_2SO_4 solution (used as an electrolyte) was purged with nitrogen gas to remove dissolved oxygen before each measurement. All PFOA removal experiments were performed in triplicates, and the variance in their results is shown as error bars or standard deviations as applicable.

2.5. Sample analysis

GC-MS (Agilent 8890 GC, Agilent 5977B MS) (Section S2) [44] and electrochemical methods with PFDT/AuNPs/GCE electrode (Section S2) [45] were used to measure the concentration of PFOA and its degradation byproducts. Figure S3 shows the calibration curve used. A fluoride combination ion selective electrode from HANNA instruments (LOD of 10 μg/L) was used to test fluoride concentration (C_F^-) in solution after electrochemical oxidation.

2.6. Data analysis

The defluorination efficiency was determined according to Eq. 2:

$$Defluorination\ efficiency = \frac{C_{F^-}}{(C_0 - C_t) \times \mathrm{n}} \times 100\% \quad (2)$$

where C_0 and C_t are the initial concentration (g/L) of PFOA in the solution and the concentration of PFOA at time t (h), respectively, C_F^- is the residual fluoride concentration (g/L) during the PFOA degradation and n = 15 for the PFOA molecule. The Electric Energy per Order (EE/O, kWh/m^3) represents the amount of electrical energy needed to decrease the concentration of a pollutant by a magnitude [46], and it is calculated by Eq. 3:

$$EEO = \frac{P \times t \times 1000}{V \times 60 \times \log\left(\frac{C_0}{C_t}\right)} \quad (3)$$

where, P is the rated power (kW), and V is the volume of solution (L).

2.7. Computational studies

All the calculations were performed using density functional theory (DFT), as implemented in ORCA software v.5.0.3 [47]. Gas-phase geometry optimizations were performed using the meta GGA hybrid TPSSh functional combined with the def2-TZVP basis set [48–50]. Dispersion effects were considered in all calculations via Grimme's D3 protocol and the Becke-Johnson (D3BJ) damping scheme [51]. A tight convergence of the wavefunction and a grid quality defgrid2 were applied. Geometry optimizations were followed by the calculation of vibrational frequencies at the TPSSh-D3/def2-TZVP/defgrid2 level of theory, the same level as optimization calculations to obtain the thermodynamic corrections to the electronic energy employing the rigid-rotor and harmonic oscillator approximations at T = 273.15 K and to evaluate that the optimized equilibrium geometries correspond to minima of the potential energy surface by the absence of imaginary frequencies. Solution state energies of all species were calculated using the universal solvation model based on solute electron density (SMD) [52], as implemented in Orca 5.0.3. The solvent cavity was generated using the gepol algorithm [53–55] as a solvent-excluded surface. The atomic radii of the default method were adjusted to H (1.250 Å), C (2.000 Å), O (1.600 Å), and F (1.682). The probe radius of water was set at 1.40 Å.

The Born-Haber thermodynamic cycle was employed to evaluate the solution state reaction Gibbs free energy of the different reduction processes studied. For the computation of reduction potentials, we employed the defining equation of the half-cell potential of an A/A^- redox couple (Eq. 4) where $\Delta G^{0,sol}$ corresponds to the solution-state reaction Gibbs free energy of the reduction process, n is the number of electrons transferred (n = 1), and F is the Faraday constant (F = 96500 C mol^{-1}). The standard reduction potential (E^0) was then determined from the half-cell potential minus the absolute half-cell potential of the reference electrode, which herein is SCE with a value of 4.681 V [56,57]

$$E^0(A/A^-) = \frac{-\Delta G^{0,sol}(A/A^-)}{nF} \quad (4)$$

Multiwfn [58] software v. 3.8 was used to calculate Hirshfeld charges to compute radical attack Fukui indexes (f^0) according to Eq. 5.

$$f_A^0 = 1/2(q_{N-1}^A - \quad q_{N+1}^A) \quad (5)$$

Where q^A corresponds to the Hirshfeld charge of atom A at the corresponding state (N is the number of electrons in the PFOA anion molecule). A plot of the f^0 Fukui function was prepared in Multiwfn 3.8 and visualized and plotted in VMD 1.9.3. [59]

3. Results and discussion

3.1. Characterization

XRD patterns of samples are shown in Fig. 1a. Pristine h-BN shows a distinct reflection at 26.50° (0 0 2) and weak reflections at 41.46° (1 0 0), 43.66° (1 0 1), and 49.99° (1 0 2). UiO-66 shows strong diffraction peaks at 7.25°, 8.44°, and 25.67° corresponding to the reflections from the (1 1 1), (0 0 2), and (0 0 6) crystal planes, respectively [60]. For samples B-1 to B-6, as the ratio of UiO-66 to h-BN increases, the diffraction peak of UiO-66 increases, while the diffraction peak of h-BN decreases.

Fig. 1(b) shows the FT-IR spectra of samples B-1 to B-6. Pristine h-BN has two strong peaks at 790 and 1375 cm^{-1} attributed to the B−N−B bending (out of plane) and the B−N ring stretch (in-plane), respectively [60]. For UiO-66, the peak at 1661 cm^{-1} is attributed to the C═O stretch, 1584 and 1395 cm^{-1} correspond to the asymmetric and symmetric stretches of O−C−O, 743 and 669 cm^{-1} are respectively attributed to O−H and C−H vibrations, and the bonds at 550 and 483 cm^{-1} are metallic oxides (Zr−O) vibrations. As the ratio of UiO-66 to h-BN increases, from samples B-1 to B-6, the IR signal of UiO-66 is enhanced, and those of h-BN are reduced.

The SEM of BN and UiO-66 are shown in Fig. 2(a) and (f), respectively. And Fig. 2(b-e) presents the SEM of UiO-66@BN materials (B-1, B-3, B-4, and B-6), respectively. The surface of BN is flat (Fig. 2a), and with UiO-66 attached, the h-BN surface becomes uneven due to the introduction of irregular intergrown crystallite polyhedra (Fig. 2f). Figure S4 shows the N_2 adsorption and desorption on the surface of the samples of UiO-66@BN and its parent materials (UiO-66 and h-BN). Their specific surface areas (SSA) are consistent with previous studies, measured via BET, and are 6.99 and 1374.13 m^2/g (Table S4), respectively [37,61]. The introduction of UiO-66 to h-BN increases their

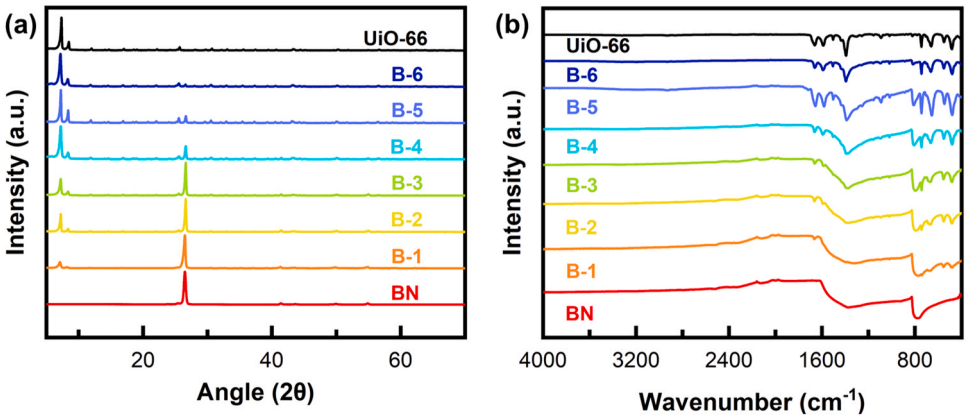

Fig. 1. (a) XRD and (b) FT-IR of BN, UiO-66, and UiO-66@BN (B-1(0.1:1), B-2 (0.2:1), B-3 (0.5:1), B-4 (1:1), B-5 (2:1), and B-6 (10:1)).

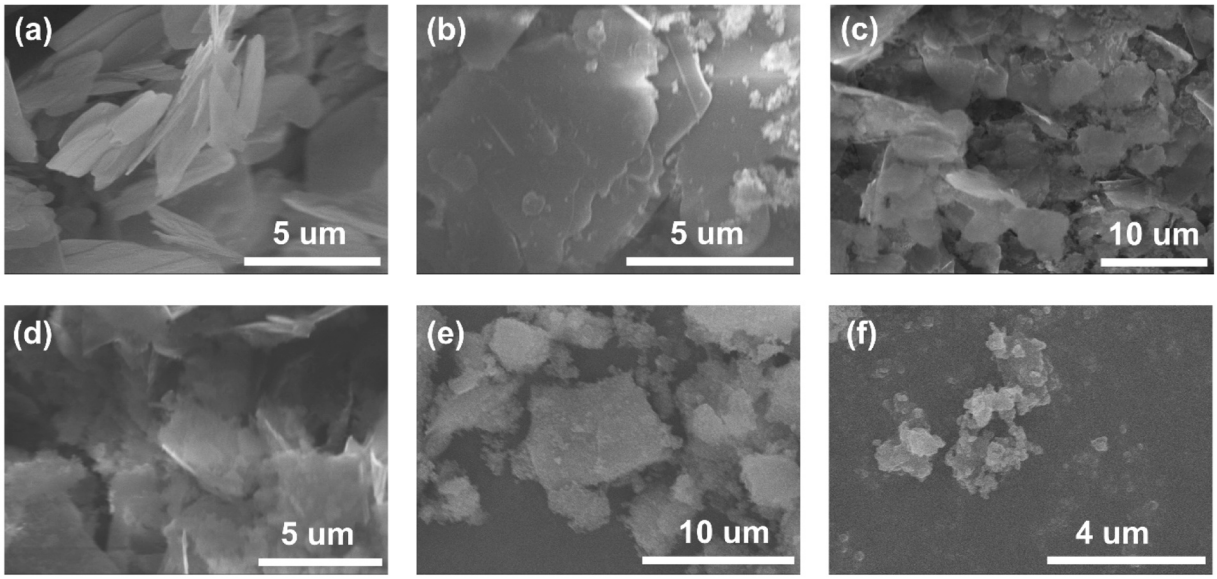

Fig. 2. Scanning Electron Micrographs of (a) h-BN, (b) B-1 (0.1:1), (c) B-3(0.5:1), (d) B-4 (1:1), (e) B-6 (10:1), (f) UiO-66.

capacity to adsorb PFOA by increasing the SSA, thereby enhancing the degradation processes.

3.2. PFOA electrochemical oxidation

Square-wave voltammetry (SWV) was used to study the oxidation of PFOA at pH 4.5, in a window potential from 0.0 V to 2.0 V *vs.* SCE. Fig. 3 shows the square wave voltammograms of (a) UiO-66, (b) pristine h-BN, and (c) B-4, with and without PFOA in 0.1 M Na_2SO_4 which was used as a supporting electrolyte. As shown in Fig. 3(a), an increase in the current response is observed in the 100 mg/L PFOA solution, compared to the blank solution, which indicates that UiO-66 enhances electron transfer during the oxidation of PFOA. Control experiments without h-BN show no PFOA oxidation response (Figure S5a). UiO-66 shows high stability in

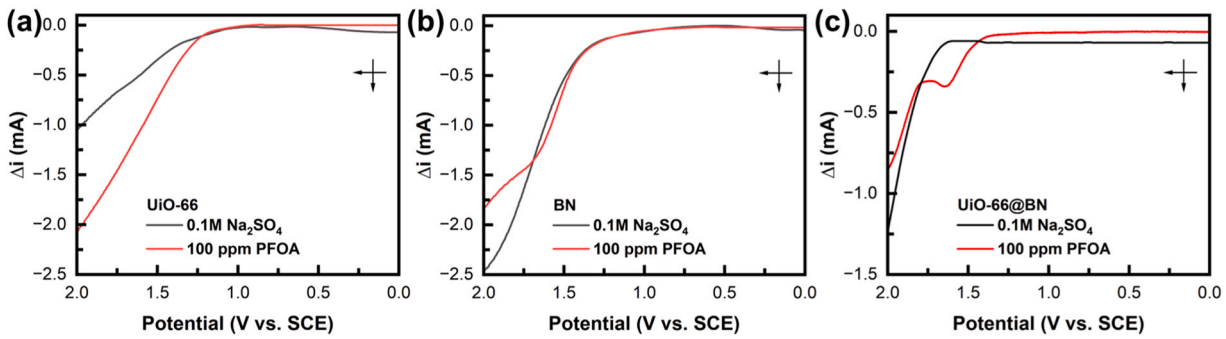

Fig. 3. Square wave voltammetry (SWV) of (a) UiO-66, showing no electrochemical response to PFOA; (b) h-BN, showing a small oxidation peak coupled to a decrease of the water oxidation (OER) current; and (c) UiO-66@BN (B-4, 1:1) showing an enhanced oxidation response to PFOA. SWV measurements were performed in 0.1 M Na_2SO_4 solution and a 100 mg/L (ppm) PFOA solution, $f = 20$ Hz and $E_{step} = 25$ mV.

electrochemical oxidation conditions, which is consistent with previous studies in electrochemical sensors [42], water-splitting electrodes [62], and pollutant oxidation electrodes [63].

Water oxidation competes with PFOA oxidation since it is thermodynamically accessible, $E^0 = 1.53$ V vs SCE at pH 4.5. The surfactant properties of PFOA are conducive to it covering the h-BN surface and hindering the access of water molecules to the anode. This effect is increased by the hydrophobic interaction of the h-BN surface and its electron-hole with the perfluorinated tail of PFOA. Fig. 3(b) shows a broad peak on the h-BN electrode at 1.60 V *vs.* SCE, whose shape is better defined with the addition of UiO-66 to the h-BN surface (B-4, Fig. 3c), confirming that PFOA is oxidized under this potential range. At 1.60 V *vs.* SCE, no redox events are observed on the blank solution, which suggests that UiO-66@BN inhibits water oxidation and improves the efficiency of PFOA oxidation via proximal sorption (and concentration) to catalytic sites. In addition, UiO-66 increases the PFOA concentration near the surface of h-BN, improving its electrode surface contact by trapping it. Figure S6 shows the CV of the UiO-66@BN (B-4) electrode in a 0.1 M Na_2SO_4 solution with and without PFOA (at pH 4.5). The current density (*j*) is 40.18 mA/cm^2. Under these conditions, it is difficult to discern the oxidation events of PFOA due to the lower sensitivity of CV versus SWV [64]. Figure S7 shows the EIS of the BN and UiO-66@BN (B-4) electrodes in 100 μg/L PFOA + 0.1 M Na_2SO_4. The impedance of B-4 is smaller than that of BN. This suggests that the introduction of UiO-66 can reduce the resistance of the electrodes, which can enhance the current response of PFOA oxidation.

Table 1 shows that the PFOA oxidation potential on UiO66@BN varies across different pH conditions. At pH 4.5, the PFOA oxidation potential is 1.65 V *vs.* SCE (Figure S5b), whereas at pH 11, the oxidation potential is 1.30 V *vs.* SCE (Figure S8d). Acidic conditions reduce the production of free radicals or intermediates, which hinder the oxidation process of PFOA since a protonated carboxyl group is less prone to Kolbe oxidation. PFOA also forms PFOA anions under basic conditions (pK_a = 3.8), facilitating the oxidation process (Figure S8) [14]. The PFOA anodic response increases with the lowering of pH (Figure S5b and S8). In strongly acidic conditions (Figure S5b and S8a), the current response increases by an order of magnitude compared to weak acidic (Figure S8b) and basic conditions (Figure S8c and S8d) [65,66]. Moreover, PFOA exists as an anion at pH values higher than 3.8 and can be oxidized to a radical ($C_nF_{2n+1}COO\bullet$) to enhance its degradation process [2,14]. The pH change of PFOA solution oxidation is shown in Table S5. There were no major fluctuations in the pH value. For instance, the initial pH is 4.52, and the measured pH is 4.87 after 3 h of electrochemical oxidation.

3.3. Selection of h-BN-based electrodes

Fig. 4 shows the results of the electrocatalytic degradation of PFOA with different synthesized electrodes at one-, two-, and three-hour intervals. High PFOA concentrations of 100 mg/L were used for electrode selection and to facilitate the mechanistic understanding of the trap-n-zap process (adsorption and electrochemical oxidation). A control blank carbon paper electrode shows no PFOA oxidation. h-BN by itself removes PFOA with a ~74.6% efficiency in 3 h. Different UiO-66:h-BN loadings (B-1(0.1:1), B-2 (0.2:1), B-3 (0.5:1), B-4 (1:1), B-5 (2:1), and B-6 (10:1)) show differences in their electrodegradation properties. B-4 (1:1) had the highest PFOA removal (93.3%) and was selected as the optimal electrode. Electrodes B-3, B-4, and B-5 have a removal rate of over 90%, likely due to the partial distribution of UiO-66 on the surface of BN. For instance, the SEM of B-3 and B-4 (Figs. 2c and 2d) shows UiO-66 aggregates and adheres to the BN surface, and the BN surface is not completely covered. That distribution can not only increase the PFOA concentration on the surface of electrodes but also leave enough available sites for BN to interact with and degrade PFOA. The SEM of B-1 and B-6 (Figs. 2b and 2e) show a larger coverage of BN by UiO-66, respectively, which likely limits the degradation process.

Table 1
Oxidation potentials of PFOA for UiO-66@BN electrode under various pH conditions.

pH	Oxidation potential (V *vs.* SCE)
3.5	2.00
4.5	1.65
6.5	1.45
9.5	1.40
11.0	1.30

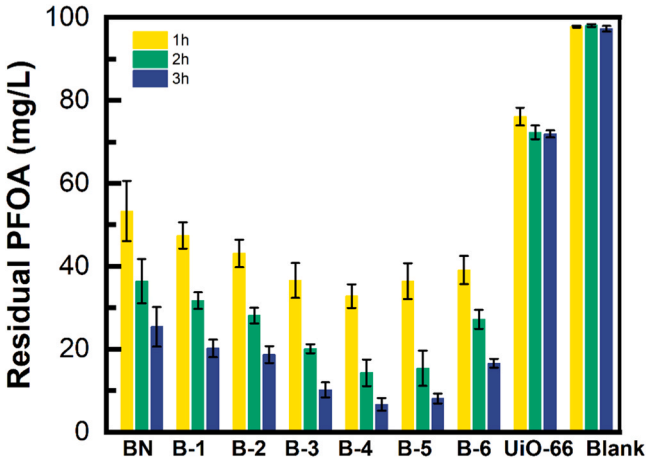

Fig. 4. PFOA oxidation by h-BN, UiO-66, UiO-66@BN (B-1(0.1:1), B-2 (0.2:1), B-3 (0.5:1), B-4 (1:1), B-5 (2:1), and B-6 (10:1)) and blank electrode (carbon paper) at different times (C_0 = 100 mg/L, pH = 4.5). Error bars represent the range of three independent measurements each.

Figure S9 shows the result of the adsorption properties of the h-BN, UiO-66, and a series of UiO-66@BN electrodes in the absence of an applied voltage. The yellow bars in Figure S9 show that less than 10% of PFOA (>90 mg/L final concentration) is adsorbed after three hours. The amount of PFOA adsorbed on UiO-66 after 3 h is 316.8 mg/g (Figure S9). This suggests that UiO-66 adsorbs PFOA by electrostatic and hydrophobic interactions, and this data is consistent with previous studies [39,40]. UiO-66 has strong adsorption properties toward PFOA with a Freundlich constant (1/n) of 0.45 [65]. Conversely, the h-BN surface has a small amount of adsorbed PFOA (see Figure S9) with a residual concentration of 98.3 mg/L after 3 h of adsorption (for 100 mg/L PFOA) [34]. The adsorption isotherms of PFOA by UiO-66@BN (1:1) are shown in Figure S10 and summarized in Table S6. The adsorption of PFOA by UiO-66 has been previously modeled by others [40] who have found a good fit for Langmuir isotherms. Upon compositing UiO-66 to the BN surface, the adsorption isotherm is less well-behaved and conforms more closely to the Freundlich model (R^2 = 0.98). The introduction of BN facilitates multilayer adsorption and increases the heterogeneous distribution of adsorbents. Using the Langmuir model, the adsorption capacity of the UiO-66@BN (1:1) is calculated to be 228 mg/g. The electrochemical surface area (ECSA, Section S4) of h-BN and UIO-66 are 14.54 cm^2 and 80.72 cm^2, respectively. The ECSA of B-4 cannot be directly estimated since the exact UiO-66 composition is unknown. However, its ECSA falls between 14.54 and 80.72 cm^2 (Figure S11). UiO-66 shows an improved PFOA adsorption under an applied voltage due to electro-adsorption (1320 mg/g within 3 h) (Fig. 4, right side) [40].

By comparing the PFOA concentration between h-BN electrochemical oxidation (25.4 mg/L, residual PFOA in Fig. 4 after 3 h) and the h-BN blank experiment (adsorption), we propose that decorated h-BN electrodes can degrade PFOA by electrocatalytic oxidation (Figure S12a). UiO-66 on the surface of h-BN enhances the oxidation of PFOA by facilitating proximity to catalytic sites and increasing the local

concentration of PFOA near the electrochemically active surface (Figure S12). Figure S12b shows that the UiO-66 modified h-BN has a higher efficiency than the sum of their individual effects, suggesting the synergistic combination of these materials to enable a "trap-n-zap" approach.

Table S7 shows the Electric Energy per Order (EE/O) values for the electrochemical oxidation of PFOA. The lower the EE/O value, the less energy is required to degrade PFOA. The electrochemical EE/O of h-BN is 22.72 kWh/m^3, while introduced UiO-66 can reduce EE/O. B-4 achieved the lowest EE/O value of all the modified BN materials with 6.1 kWh/m^3. Table 2 shows the compilation of various studies on PFOA electrochemical oxidation using different electrode materials like BDD and Ti-based electrodes. Overall, h-BN-based electrodes demonstrate potential for practical PFOA electrochemical oxidation. A comparison of PFOA degradation using h-BN-based materials through electrochemical and photochemical oxidation is shown in Table S8.

3.4. Electrochemical oxidation of PFOA at environmentally relevant concentrations

Figure S13(a) shows the results of the electrochemical oxidation of PFOA by pristine h-BN electrode in 3 h at an initial environmentally-relevant PFOA concentration of 100 μg/L, with a removal efficiency of 67.5%. Fig. 5 illustrates the efficiency of PFOA removal and defluorination at concentrations of 100 μg/L and 100 mg/L by UiO-66@BN (B-4). The defluorination efficiency indicates that PFOA is not completely oxidized, suggesting that shorter chains are preserved during the PFOA degradation process. Within the first 10 min, a lower PFOA concentration (100 μg/L) exhibits a sharp decrease due to electroabsorption. After equilibrium, the removal rate of PFOA decreases. After 3 h of electrochemical oxidation, the removal efficiencies for concentrations of 100 μg/L and mg/L are 99.5% and 93.3%, respectively, and their defluorination efficiencies are 69.7% and 48.8%, respectively. At even lower initial PFOA concentrations (10 μg/L, Figure S13b), B-4 shows a sharp decrease in PFOA concentration in the first 15 min, with over 99% removal observed within 2 h. The introduction of UiO-66 to h-BN significantly enhances PFOA degradation through the trap-n-zap process, and it may also result in adsorption of the released F^- [67], which would conservatively decrease the estimated defluorination efficiency.

When contemplating the practical application of UiO-66@BN electrodes, it is important to understand the conditions (composition and concentration) of the contaminated media, which significantly affect the performance and efficacy of electrochemical treatment methods [72]. Due to the flexibility and stability of the UiO-66@BN material, it can be utilized in various electrode designs, including plane and cylindrical electrodes. These h-BN materials can be used as anodes in traditional tank and bi-polar cells, as well as advanced setups like packed bed electrochemical reactors and bi-polar trickle tower electrochemical reactors [73].

Table 2
Comparison of energy per order (EE/O, kWh/m^3) values for the electrochemical oxidation of PFOA.

Anode	Current Density mA/cm^2	Electric Energy per Order (EE/O) kWh/m^3	Reference
h-BN	51	22.7	This study
B-4 (1:1)	40	6.1	This study
BDD (flow-through)	50	8.0	[68]
BDD (groundwater)	15	40.0	[69]
Ti_4O_7	5	18.5	[70]
Ti_4O_7 (membrane)	-	5	[23]
Ti_4O_7 (microporous)	5	14.2	[28]
Ti-SnO_2-Sb	5	6.75	[71]

3.5. Reusability and stability

To assess the stability of the electrodes, 5 cycles of PFOA electrochemical oxidation have been conducted (Fig. 6a). The initial current densities remained stable for each cycle at around 40–50 mA/cm^2. The current density is stable during the first 0.5 h because the PFCA concentration is relatively stable on the electrode surface. After 0.5 h, the concentration of PFOA decreases (Fig. 5a), and the current density decreases, approaching a value close to zero (3 mA/cm^2) after 2 h. These changes also prove the limited occurrence of water oxidation (OER) on UiO-66@BN electrodes under experimental conditions (pH 4.5 and 2.2 V *vs.* SCE). The Tafel plot of UiO-66@BN is shown in Figure S15, and the Tafel slope is 125 mV/dec. Fig. 6b shows the FT-IR spectra of the electrodes after 5 cycles. The spectra exhibit peaks corresponding to both BN (790 cm^{-1}, B−N−B) and UiO-66 (1584 and 1395 cm^{-1}, O−C−O), which indicates the stability of electrodes after cycles. No discernible PFAS (1653 cm^{-1}, C−F) [74] or water (3300 cm^{-1}, H−O) peaks were measured on naturally dried electrodes after PFOA oxidation.

Figures S14 and S15 show the SEM images, elemental mapping analysis, and EDS analysis of the UiO-66@BN (B-4) electrode before and after the electrochemical oxidation of PFOA. The surface structure of UiO-66@BN (B-4) remains unchanged (Figure S14), and there is no significant alteration in the element ratio of N, Zr, and F (from BN, UiO-66, and Nafion, respectively) as shown in Figures S15. Those suggest that the electrode maintains stability under the electrochemical conditions required for PFOA oxidation.

3.6. Mechanism

Fig. 7 shows the GC-MS analysis results of a PFOA solution after one hour of electrochemical oxidation with UiO-66@BN. The response peak of PFOA (C8) decreases, while short-chain PFAS such as C7, C6, and C5 are observed. The appearance of shorter chains like C6 and C5 suggests that once the oxidation of PFOA molecules begins, the degradation of PFOA continues, resulting in the formation of shorter PFAS chains. These processes may occur simultaneously with the oxidation of PFOA. This observation is consistent with our defluorination result and previous studies on PFOA oxidation. [75,76]

Figure S17 shows the electrochemical oxidation of 100 mg/L PFOA by BN electrode under different electrolytes (SO_4^{2-}, Cl^-, PO_4^{3-}, and ClO_4^-) for 1 h. The residual concretions in PO_4^{3-} and ClO_4^-) are close to that in SO_4^{2-}, while in Cl^- is much higher than that in SO_4^{2-}. To investigate the impact of Cl^-, electrolysis experiments with 0.1 M KCl as the electrolyte was used instead of Na_2SO_4. UiO-66@BN can also oxidize Cl^- (Figure S18a) at around 1.70 V (*vs.* SCE). However, as the concentration of PFOA increases, the electrochemical response of Cl^- diminishes and is replaced by PFOA oxidation. Therefore, the preferential oxidation of this material is PFOA $\geq Cl^- > H_2O$, likely due to the surfactant properties of PFOA. Oxidation of Cl^- to Cl_2 is a competing reaction that decreases PFOA oxidation efficiency. [77,78] Figure S18 (b) shows the oxidation of PFOA with 0.1 M KCl as the electrolyte for 3 h. The concentration of residual PFOA is around 48.2 mg/L, which is higher than the residual concentration in 0.1 M Na_2SO_4 electrolyte (6.7 mg/L). This is because Cl^- can act as a scavenger of free radicals, hindering the oxidation of PFOA at high potential (> 2.0 V *vs.* SCE). [14] When PFOA oxidation occurs in the presence of Cl^-, the free radicals may react with Cl^- to form Cl•, which can generate chlorinated byproducts. [78] The use of Na_2SO_4 avoids these competing reactions.

Figure S19 shows the potential oxidation mechanism (decarboxylation–hydroxylation–elimination–hydrolysis, DHEH pathway) of perfluorinated carboxylic acids (PFCA), and their equations are shown in SI (Section S6). [2] The oxidation starts with the formation of $C_nF_{2n+1}COO•$, which can be formed from $C_nF_{2n+1}COO^-$ directly by an

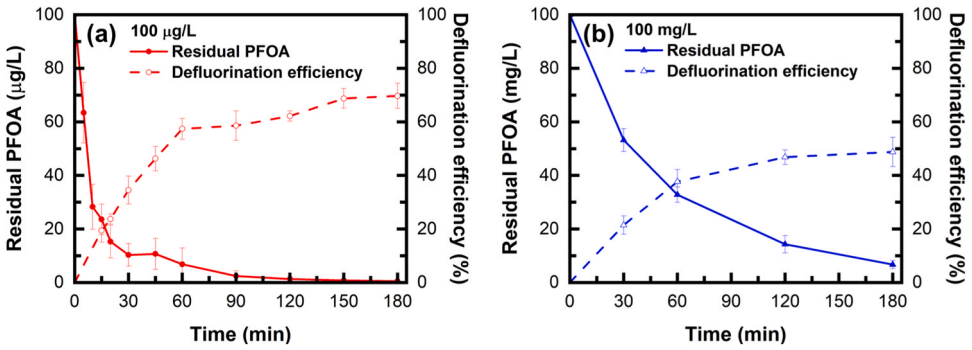

Fig. 5. PFOA degradation and defluorination efficiency changes in (a) 100 μg/L and (b) 100 mg/L. Error bars represent the range of three independent measurements each.

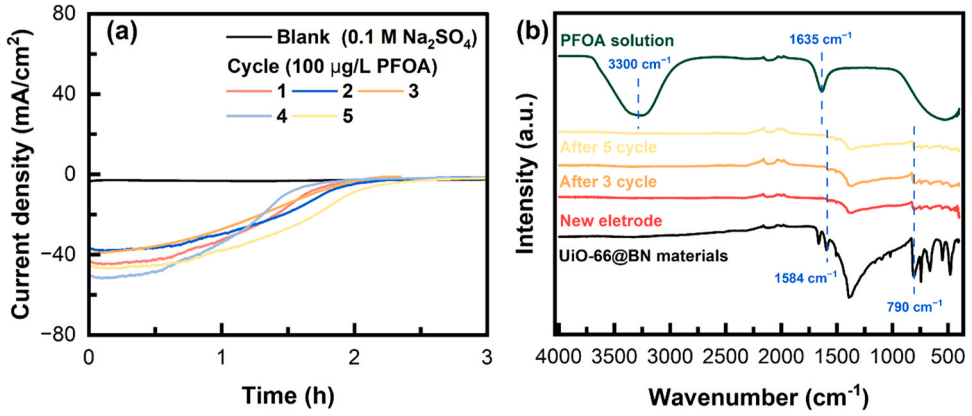

Fig. 6. (a) Stability of electrodes for 5 100 μg/L PFOA electrochemical oxidation cycles, and (b) FT-IR of electrodes after 5 cycles.

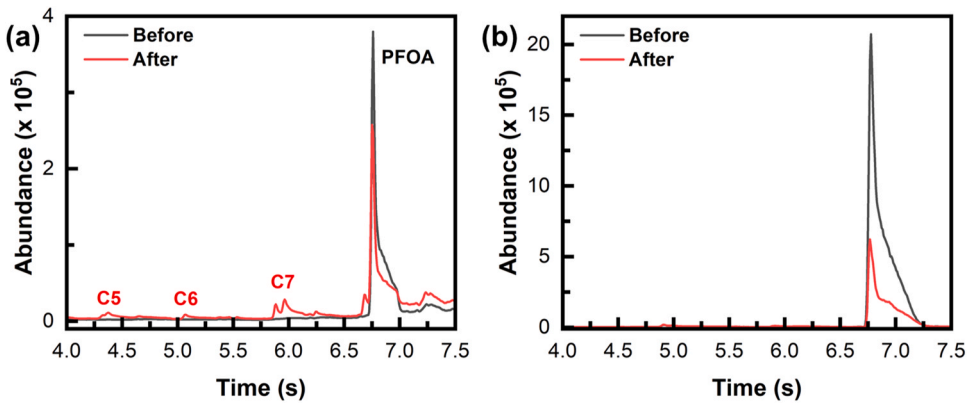

Fig. 7. GC-MS Chromatograms before and after electrochemical oxidation via UiO-66@BN. (a) Detection of PFAS byproducts. Shorter chain PFAS (C7, C6, and C5) were observed after electrochemical oxidation. (b) Decreasing abundance/concentration change for PFOA after electrochemical oxidation.

electrocatalytically generated, hydrophobic electron-hole on the h-BN anode. [2,79,80] $C_nF_{2n+1}COO\bullet$ radical is unstable and loses one CF_2 unit by decarboxylation, hydrolysis, and defluorination events, producing a shorter chain PFCA and continuing in a new cycle beginning with further oxidation at the anode.

3.7. Computational studies

DFT calculations have been proven helpful for studying the degradation mechanisms of fluorinated compounds [81–83]. The mechanism between PFOA oxidation and BN has been reported in a previous study [34,84]. In this context, we explored the proposed potential mechanism for PFOA electrochemical oxidation using DFT calculations (Fig. 8b). Our calculations suggest that an overpotential of 2.11 V vs. SHE (1.87 V vs. SCE) is required for the formation of $C_7F_{15}COO\bullet$ radical, which is the rate-limiting step. The calculated overpotential of around 1.87 V agrees with the observed experimental overpotential for this oxidation (2.00 – 1.65 V *vs.* SCE in the pH 3.5 – 4.5 pH range, and the pKa of PFOA is 3.8). Calculated fukui indexes (Fig. 8a – bottom) and electron density difference distributions (Fig. 8a – top) representing the radical attack ($f[^0]$) indicate that the highest probability for radical attacks in PFOA is centered on the -COO^- functional group resulting in its decarboxylation in a further step. After PFOA oxidation, the reaction proceeds via a thermodynamically favorable pathway. Decarboxylation of the

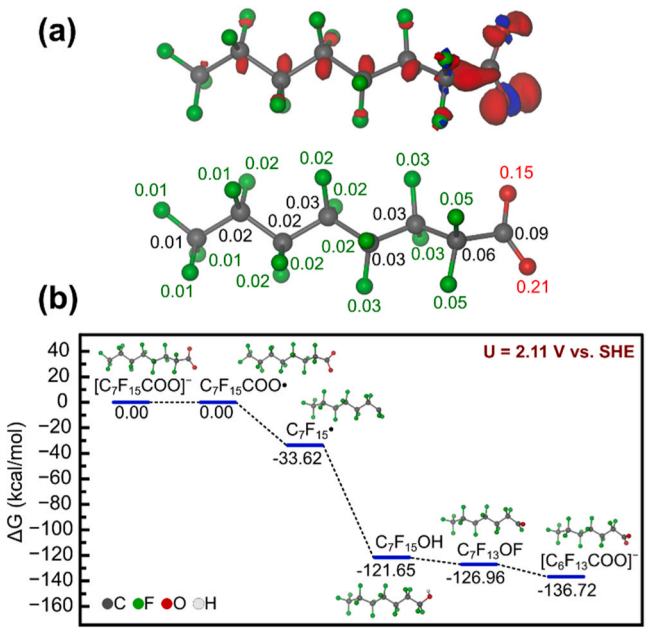

Fig. 8. (a) Calculated electron density distributions (top) and Fukui indexes (bottom) for radical attack (f^0) at the PFOA molecule. Red lobes represent the accumulation of electron density while the blue lobes indicate depletion (b) Computational profile of the solution state Gibbs free energy (kcal/mol) for the electro-oxidation of $C_7F_{15}COO^-$ at U = 2.11 V vs SHE.

$C_7F_{15}COO\bullet$ radical generates CO_2 and $C_7F_{15}\bullet$ with a ΔG_r = −33.62 kcal/mol. The unstable $C_7F_{15}\bullet$ radical is further stabilized by the reaction with •OH to generate a $C_5F_{15}OH$ molecule (ΔG_r = −88.03 kcal/mol). In the first defluorination event, $C_7F_{13}OF$ is formed (ΔG_r = –5.31 kcal/mol), which is followed by the hydrolysis of the latter to form $C_6F_{13}COO^-$ (ΔG_r = –9.76 kcal/mol). This result is consistent with previous studies [82]. Shorter chain PFAS will also likely undergo the same decarboxylation/ defluorination cycle, eliminating a CF_2 unit in each cycle.

4. Conclusion

This study focuses on the electrocatalytic oxidation of PFOA using UiO-66 modified h-BN, an inexpensive and widely available material. We demonstrated that h-BN-based electrodes can electrocatalytically oxidize PFOA to $C_7F_{15}COO\bullet$ radical and shorter chain PFAS with mild voltages. Adding UiO-66 onto the surface of h-BN enhances the adsorption of PFOA onto the electrode surface and improves the kinetics of the PFOA degradation by exploiting a trap-n-zap approach. UiO-66@BN electrodes exhibit efficient PFOA removal at environmentally relevant concentrations, which is further optimized at pH 4.5. After 3 h of electrocatalytic oxidation, the removal and defluorination efficiencies of UiO-66@BN for 100 μg/L PFOA are 99.5% and 69.7%, respectively. This research contributes to developing more sustainable technologies for removing PFAS from the environment, addressing the urgent health and environmental concerns associated with these persistent pollutants. Future studies should focus on further optimizing the UiO-66@BN electrode and exploring the applicability of this method on a larger scale. Additionally, the environmental impacts of the degradation byproducts should be thoroughly assessed to ensure the overall safety and sustainability of the electrochemical treatment process.

CRediT authorship contribution statement

Ahsan Habib: Writing – review & editing, Methodology, Formal analysis. **Pedro J.J. Alvarez:** Writing – review & editing, Funding acquisition, Conceptualization. **Dino Villagran:** Writing – review & editing, Supervision, Project administration, Funding acquisition, Conceptualization. **Wen-Yee Lee:** Writing – review & editing, Methodology, Formal analysis. **Michael S. Wong:** Writing – review & editing, Conceptualization. **Juan Francisco López:** Writing – review & editing, Validation, Methodology, Data curation. **Christian Sandoval-Pauker:** Writing – review & editing, Writing – original draft, Software. **Sheng Yin:** Writing – review & editing, Writing – original draft, Validation, Software, Methodology, Formal analysis, Data curation, Conceptualization. **Jonathan J. Calvillo Solís:** Writing – review & editing, Methodology. **Sarah Glass:** Writing – review & editing, Conceptualization.

Declaration of Competing Interest

The authors declare that they have no known competing financial interests or personal relationships that could have appeared to influence the work reported in this paper.

Data availability

Data will be made available on request.

Acknowledgments

We are grateful to the NSF Nanosystems Engineering Research Center for Nanotechnology-Enabled Water Treatment (NEWT) (ERC-1449500), the Welch Foundation under award number AH-2083-20210327. WYL and AH acknowledge funding from the National Cancer Institute of the National Institutes of Health (NCI-NIH) under award number SC1CA245675. The authors thank UTEP HPC JAKAR Cluster for the computational resources provided free of charge. M.S.W. acknowledges additional support from the Strategic Environmental Research and Development Program (SERDP) award ER 22-3258 and NSF (TI-2243301 and TI-2314154).

Appendix A. Supporting information

Supplementary data associated with this article can be found in the online version at doi:10.1016/j.apcatb.2024.124136.

References

[1] R. Dhore, G.S. Murthy, Per/polyfluoroalkyl substances production, applications and environmental impacts, Bioresour. Technol. *341* (2021) 125808.
[2] S. Yin, D. Villagrán, Design of nanomaterials for the removal of per-and poly-fluoroalkyl substances (PFAS) in water: strategies, mechanism, challenges, and opportunities, Sci. Total Environ. (2022) 154939.
[3] G.R. Johnson, M.L. Brusseau, K.C. Carroll, G.R. Tick, C.M. Duncan, Global distributions, source-type dependencies, and concentration ranges of per-and polyfluoroalkyl substances in groundwater, Sci. Total Environ. *841* (2022) 156602.
[4] J.L. Sims, K.M. Stroski, S. Kim, G. Killeen, R. Ehalt, M.F. Simcik, B.W. Brooks, Global occurrence and probabilistic environmental health hazard assessment of per-and polyfluoroalkyl substances (PFASs) in groundwater and surface waters, Sci. Total Environ. *816* (2022) 151535.
[5] P. Zareitalabad, J. Siemens, M. Hamer, W. Amelung, Perfluorooctanoic acid (PFOA) and perfluorooctanesulfonic acid (PFOS) in surface waters, sediments, soils and wastewater–a review on concentrations and distribution coefficients, Chemosphere *91* (6) (2013) 725–732.
[6] F. Xiao, M.F. Simcik, T.R. Halbach, J.S. Gulliver, Perfluorooctane sulfonate (PFOS) and perfluorooctanoate (PFOA) in soils and groundwater of a US metropolitan area: migration and implications for human exposure, Water Res *72* (2015) 64–74.
[7] S.M. Bartell, V.M. Vieira, Critical review on PFOA, kidney cancer, and testicular cancer, J. Air Waste Manag. Assoc. *71* (6) (2021) 663–679.
[8] F. Coperchini, O. Awwad, M. Rotondi, F. Santini, M. Imbriani, L. Chiovato, Thyroid disruption by perfluorooctane sulfonate (PFOS) and perfluorooctanoate (PFOA), J. Endocrinol. Invest. *40* (2017) 105–121.
[9] K. Steenland, S. Kugathasan, D.B. Barr, PFOA and ulcerative colitis, Environ. Res. *165* (2018) 317–321.
[10] Holtcamp, W. Pregnancy-Induced Hypertension "Probably Linked" to PFOA Contamination, 2012.
[11] European CommissionCommission Delegated Regulation (EU) 2020/784 of 8 April 2020 Amending Annex I to Regulation (EU) 2019/1021 of the European Parliament and of the Council as Regards the Listing of Perfluorooctanoic Acid (PFOA), Its Salts and PFOA-Related Compounds Vol 188 Off. J. Eur. Union2020, ,

Commission Delegated Regulation (EU) /784 of 8 April 2020 Amending Annex I to Regulation (EU) 2019/1021 of the European Parliament and of the Council as Regards the Listing of Perfluorooctanoic Acid (PFOA), Its Salts and PFOA-Related Compounds20201–5.
[12] U. EPA, Emerging contaminants-perfluorooctane sulfonate (PFOS) and perfluorooctanoic acid (PFOA), Emerg. Contam. Fact. Sheet–PFOS PFOA (2012).
[13] E.B. Esfahani, F.A. Zeidabadi, S. Zhang, M. Mohseni, Photochemical/catalytic oxidative/reductive decomposition of per-and polyfluoroalkyl substances (PFAS), decomposition mechanisms and effects of key factors: a review, Environ. Sci. Water Res. Technol. (2022).
[14] S.C.E. Leung, P. Shukla, D. Chen, E. Eftekhari, H. An, F. Zare, N. Ghasemi, D. Zhang, N.-T. Nguyen, Q. Li, Emerging technologies for PFOS/PFOA degradation: a review, Sci. Total Environ. (2022) 153669.
[15] S. Das, A. Ronen, A review on removal and destruction of per-and polyfluoroalkyl substances (PFAS) by novel membranes, Membranes *12* (7) (2022) 662.
[16] J. Wang, Z. Lin, X. He, M. Song, P. Westerhoff, K. Doudrick, D. Hanigan, Critical review of thermal decomposition of per-and polyfluoroalkyl substances: mechanisms and implications for thermal treatment processes, Environ. Sci. Technol. *56* (9) (2022) 5355–5370.
[17] S. Garcia-Segura, A.B. Nienhauser, A.S. Fajardo, R. Bansal, C.L. Conrad, J. D. Fortner, M. Marcos-Hernández, T. Rogers, D. Villagran, M.S. Wong, Disparities between experimental and environmental conditions: research steps toward making electrochemical water treatment a reality, Curr. Opin. Electrochem. *22* (2020) 9–16.
[18] S. Sharma, N.P. Shetti, S. Basu, M.N. Nadagouda, T.M. Aminabhavi, Remediation of PEr-and Polyfluoroalkyls (PFAS) via electrochemical methods, Chem. Eng. J. *430* (2022) 132895.
[19] J.J.C. Solis, A. Castillo, S. Yin, C. Sandoval-Pauker, N. Ocuane, D. Puerto-Diaz, N. Jafari, D. Villagrán, Molecular inspired electrocatalyst materials for environmental remediation, Inorg. Chem. Front. (2023).
[20] J. Radjenovic, N. Duinslaeger, S.S. Avval, B.P. Chaplin, Facing the challenge of poly- and perfluoroalkyl substances in water: is electrochemical oxidation the answer, Environ. Sci. Technol. *54* (23) (2020) 14815–14829, https://doi.org/10.1021/acs.est.0c06212.
[21] Q. Zhuo, J. Wang, J. Niu, B. Yang, Y. Yang, Electrochemical oxidation of perfluorooctane sulfonate (PFOS) substitute by modified boron doped diamond (BDD) anodes, Chem. Eng. J. *379* (2020) 122280.
[22] D. Huang, K. Wang, J. Niu, C. Chu, S. Weon, Q. Zhu, J. Lu, E. Stavitski, J.-H. Kim, Amorphous Pd-loaded Ti4O7 electrode for direct anodic destruction of perfluorooctanoic acid, Environ. Sci. Technol. *54* (17) (2020) 10954–10963.
[23] T.X.H. Le, H. Haflich, A.D. Shah, B.P. Chaplin, Energy-efficient electrochemical oxidation of perfluoroalkyl substances using a Ti4O7 reactive electrochemical membrane anode, Environ. Sci. Technol. Lett. *6* (8) (2019) 504–510.
[24] H. Lin, J. Niu, S. Ding, L. Zhang, Electrochemical degradation of perfluorooctanoic acid (PFOA) by Ti/SnO2–Sb, Ti/SnO2–Sb/PbO2 and Ti/SnO2–Sb/MnO2 anodes, Water Res *46* (7) (2012) 2281–2289.
[25] Q. Zhuo, S. Deng, B. Yang, J. Huang, G. Yu, Efficient electrochemical oxidation of perfluorooctanoate using a Ti/SnO2-Sb-Bi anode, Environ. Sci. Technol. *45* (7) (2011) 2973–2979.
[26] Z. Xu, Y. Yu, H. Liu, J. Niu, Highly efficient and stable Zr-doped nanocrystalline PbO2 electrode for mineralization of perfluorooctanoic acid in a sequential treatment system, Sci. Total Environ. *579* (2017) 1600–1607.
[27] S. Sukeesan, N. Boontanon, S.K. Boontanon, Improved electrical driving current of electrochemical treatment of per-and polyfluoroalkyl substances (PFAS) in water using boron-doped diamond anode, Environ. Technol. Innov. *23* (2021) 101655.
[28] H. Lin, J. Niu, S. Liang, C. Wang, Y. Wang, F. Jin, Q. Luo, Q. Huang, Development of macroporous magnéli phase Ti4O7 ceramic materials: as an efficient anode for mineralization of poly-and perfluoroalkyl substances, Chem. Eng. J. *354* (2018) 1058–1067.
[29] N. Duinslaeger, J. Radjenovic, Electrochemical degradation of per-and polyfluoroalkyl substances (PFAS) using low-cost graphene sponge electrodes, Water Res *213* (2022) 118148.
[30] C. Zhang, J. Tang, C. Peng, M. Jin, Degradation of perfluorinated compounds in wastewater treatment plant effluents by electrochemical oxidation with nano-ZnO coated electrodes, J. Mol. Liq. *221* (2016) 1145–1150.
[31] M.A. Assi, M.N.M. Hezmee, M.Y.M. Sabri, M.A. Rajion, The Detrimental Effects of Lead on Human and Animal Health, Vet. World *9* (6) (2016) 660.
[32] E.A. Tin Ostrakhovitch, Handbook on the Toxicology of Metals, Elsevier, 2022, pp. 807–856.
[33] J. Radjenovic, D.L. Sedlak, Challenges and opportunities for electrochemical processes as next-generation technologies for the treatment of contaminated water, Environ. Sci. Technol. *49* (19) (2015) 11292–11302.
[34] L. Duan, B. Wang, K. Heck, S. Guo, C.A. Clark, J. Arredondo, M. Wang, T.P. Senftle, P. Westerhoff, X. Wen, Y. Song, M.S. Wong, Efficient photocatalytic PFOA degradation over boron nitride, Environ. Sci. Technol. Lett. *7* (8) (2020) 613–619, https://doi.org/10.1021/acs.estlett.0c00434.
[35] A. Serrà, L. Philippe, F. Perreault, S. Garcia-Segura, Photocatalytic treatment of natural waters. reality or hype? The case of cyanotoxins remediation, Water Res *188* (2021) 116543.
[36] S. Angizi, M. Khalaj, S.A.A. Alem, A. Pakdel, M. Willander, A. Hatamie, A. Simchi, Towards the two-dimensional hexagonal boron nitride (2D h-BN) electrochemical sensing platforms, J. Electrochem. Soc. *167* (12) (2020) 126513.
[37] N. Kostoglou, K. Polychronopoulou, C. Rebholz, Thermal and chemical stability of hexagonal boron nitride (h-BN) nanoplatelets, Vacuum *112* (2015) 42–45.
[38] M. Qiu, H. Jia, C. Lan, H. Liu, S. Fu, An enhanced kinetics and ultra-stable zinc electrode by functionalized boron nitride intermediate layer engineering, Energy Storage Mater. *45* (2022) 1175–1182.
[39] K. Sini, D. Bourgeois, M. Idouhar, M. Carboni, D. Meyer, Metal–organic framework sorbents for the removal of perfluorinated compounds in an aqueous environment. N. J. Chem. *42* (22) (2018) 17889–17894.
[40] K. Sini, D. Bourgeois, M. Idouhar, M. Carboni, D. Meyer, Metal-organic frameworks cavity size effect on the extraction of organic pollutants, Mater. Lett. *250* (2019) 92–95.
[41] R. Li, S. Alomari, T. Islamoglu, O.K. Farha, S. Fernando, S.M. Thagard, T.M. Holsen, M. Wriedt, Systematic study on the removal of per- and polyfluoroalkyl substances from contaminated groundwater using metal–organic frameworks, Environ. Sci. Technol. *55* (22) (2021) 15162–15171, https://doi.org/10.1021/acs.est.1c03974.
[42] Q. Tian, S. Chen, M. Shi, T. Gao, M. Zhang, C. Liao, X. Li, Q. Dong, C. Wang, Fluorine-functionalized MOF modified GCE for highly sensitive electrochemical detection of persistent pollutant perfluorooctanoic acid, Sens. Actuators B Chem. *404* (2024) 135309.
[43] M. Kandiah, M.H. Nilsen, S. Usseglio, S. Jakobsen, U. Olsbye, M. Tilset, C. Larabi, E.A. Quadrelli, F. Bonino, K.P. Lillerud, Synthesis and stability of tagged UiO-66 Zr-MOFs, Chem. Mater. *22* (24) (2010) 6632–6640.
[44] A. Habib, E.N. Landa, K.L. Holbrook, W.S. Walker, W.-Y. Lee, Rapid, efficient, and green analytical technique for determination of fluorotelomer alcohol in water by stir bar sorptive extraction, Chemosphere (2023) 139439.
[45] J.J. Calvillo Solís, S. Yin, M. Galicia, M.S. Ersan, P. Westerhoff, D. Villagrán, "Forever chemicals" detection: A selective nano-enabled electrochemical sensing approach for perfluorooctanoic acid (PFOA), Chemical Engineering Journal (2024) 151821, https://doi.org/10.1016/j.cej.2024.151821. In Press.
[46] O. Keen, J. Bolton, M. Litter, K. Bircher, T. Oppenländer, Standard reporting of electrical energy per order (EEO) for UV/H2O2 reactors (IUPAC technical report), Pure Appl. Chem. *90* (9) (2018) 1487–1499.
[47] F. Neese, The ORCA Program System, Wiley Interdiscip. Rev. Comput. Mol. Sci. *2* (1) (2012) 73–78, https://doi.org/10.1002/wcms.81.
[48] J. Tao, J.P. Perdew, V.N. Staroverov, G.E. Scuseria, Climbing the density functional ladder: nonempirical meta–generalized gradient approximation designed for molecules and solids, Phys. Rev. Lett. *91* (14) (2003) 146401, https://doi.org/10.1103/PhysRevLett.91.146401.
[49] V.N. Staroverov, G.E. Scuseria, J. Tao, J.P. Perdew, Comparative assessment of a new nonempirical density functional: molecules and hydrogen-bonded complexes, J. Chem. Phys. *119* (23) (2003) 12129–12137, https://doi.org/10.1063/1.1626543.
[50] V.N. Staroverov, G.E. Scuseria, J. Tao, J.P. Perdew, Erratum: "comparative assessment of a new nonempirical density functional: molecules and hydrogen-bonded complexes" [J. Chem. Phys. 119, 12129 (2003), J. Chem. Phys. *121* (22) (2004) 11507, https://doi.org/10.1063/1.1795692.
[51] S. Grimme, J. Antony, S. Ehrlich, H. Krieg, A consistent and accurate ab initio parametrization of density functional dispersion correction (DFT-D) for the 94 elements H-Pu, J. Chem. Phys. *132* (15) (2010) 154104, https://doi.org/10.1063/1.3382344.
[52] A.V. Marenich, C.J. Cramer, D.G. Truhlar, Universal solvation model based on solute electron density and on a continuum model of the solvent defined by the bulk dielectric constant and atomic surface tensions, J. Phys. Chem. B *113* (18) (2009) 6378–6396, https://doi.org/10.1021/jp810292n.
[53] J.L. Pascual-Ahuir, E. Silla, GEPOL: an improved description of molecular surfaces. I. building the spherical surface set, J. Comput. Chem. *11* (9) (1990) 1047–1060, https://doi.org/10.1002/jcc.540110907.
[54] E. Silla, I. Tuñón, J.L. Pascual-Ahuir, GEPOL: an improved description of molecular surfaces II. computing the molecular area and volume, J. Comput. Chem. *12* (9) (1991) 1077–1088, https://doi.org/10.1002/jcc.540120905.
[55] J.L. Pascual-ahuir, E. Silla, I. Tuñon, GEPOL: an improved description of molecular surfaces. III. A new algorithm for the computation of a solvent-excluding surface, J. Comput. Chem. *15* (10) (1994) 1127–1138, https://doi.org/10.1002/jcc.540151009.
[56] S. Trasatti, The Absolute electrode potential: an explanatory note (Recommendations 1986), Pure Appl. Chem. *58* (7) (1986) 955–966, https://doi.org/10.1351/pac198658070955.
[57] A.A. Isse, A. Gennaro, Absolute potential of the standard hydrogen electrode and the problem of interconversion of potentials in different solvents, J. Phys. Chem. B *114* (23) (2010) 7894–7899, https://doi.org/10.1021/jp100402x.
[58] T. Lu, F. Chen, Multiwfn: a multifunctional wavefunction analyzer, J. Comput. Chem. *33* (5) (2012) 580–592, https://doi.org/10.1002/jcc.22885.
[59] W. Humphrey, A. Dalke, K. Schulten, VMD: visual molecular dynamics, J. Mol. Graph. *14* (1) (1996) 33–38.
[60] H. Harrison, J.T. Lamb, K.S. Nowlin, A.J. Guenthner, K.B. Ghiassi, A.D. Kelkar, J. R. Alston, Quantification of hexagonal boron nitride impurities in boron nitride nanotubes via FTIR spectroscopy, Nanoscale Adv. *1* (5) (2019) 1693–1701.
[61] F. Ahmadijokani, H. Molavi, M. Rezakazemi, S. Tajahmadi, A. Bahi, F. Ko, T. M. Aminabhavi, J.-R. Li, M. Arjmand, UiO-66 metal–organic frameworks in water treatment: a critical review. Prog. Mater. Sci. *125* (2022) 100904.
[62] M. Ali, E. Pervaiz, O. Rabi, Enhancing the overall electrocatalytic water-splitting efficiency of Mo $_2$ C nanoparticles by forming hybrids with UiO-66 MOF, ACS Omega *6* (50) (2021) 34219–34228, https://doi.org/10.1021/acsomega.1c03115.
[63] B. Jiang, F. Liu, Y. Pan, Y. Tan, C. Shuang, A. Li, Preparation of graphite-UiO-66 (Zr)/Ti electrode for efficient electrochemical oxidation of tetracycline in water, Plos One *17* (8) (2022) e0271075.

[64] M. Rkik, M.B. Brahim, Y. Samet, Electrochemical determination of levofloxacin antibiotic in biological samples using boron doped diamond electrode, J. Electroanal. Chem. *794* (2017) 175–181.
[65] C.A. Clark, K.N. Heck, C.D. Powell, M.S. Wong, Highly defective UiO-66 materials for the adsorptive removal of perfluorooctanesulfonate, ACS Sustain. Chem. Eng. *7* (7) (2019) 6619–6628.
[66] X. Li, H. Zhang, P. Wang, J. Hou, J. Lu, C.D. Easton, X. Zhang, M.R. Hill, A. W. Thornton, J.Z. Liu, Fast and selective fluoride ion conduction in sub-1-nanometer metal-organic framework channels, Nat. Commun. *10* (1) (2019) 2490.
[67] K.-Y.A. Lin, Y.-T. Liu, S.-Y. Chen, Adsorption of fluoride to UiO-66-NH2 in water: stability, kinetic, isotherm and thermodynamic studies, J. Colloid Interface Sci. *461* (2016) 79–87.
[68] V.Y. Maldonado, G.M. Landis, M. Ensch, M.F. Becker, S.E. Witt, C.A. Rusinek, A flow-through cell for the electrochemical oxidation of perfluoroalkyl substances in landfill leachates, J. Water Process Eng. *43* (2021) 102210.
[69] C.E. Schaefer, C. Andaya, A. Burant, C.W. Condee, A. Urtiaga, T.J. Strathmann, C. P. Higgins, Electrochemical treatment of perfluorooctanoic acid and perfluorooctane sulfonate: insights into mechanisms and application to groundwater treatment, Chem. Eng. J. *317* (2017) 424–432.
[70] Y. Wang, H. Shi, C. Li, Q. Huang, Electrochemical degradation of perfluoroalkyl acids by titanium suboxide anodes, Environ. Sci. Water Res. Technol. *6* (1) (2020) 144–152.
[71] M. Chen, C. Wang, Y. Wang, X. Meng, Z. Chen, W. Zhang, G. Tan, Kinetic, mechanism and mass transfer impact on electrochemical oxidation of MIT using Ti-enhanced nanotube arrays/SnO2-Sb anode, Electrochim. Acta *323* (2019) 134779.
[72] S. Garcia-Segura, X. Qu, P.J. Alvarez, B.P. Chaplin, W. Chen, J.C. Crittenden, Y. Feng, G. Gao, Z. He, C.-H. Hou, Opportunities for nanotechnology to enhance electrochemical treatment of pollutants in potable water and industrial wastewater–a perspective, Environ. Sci. Nano *7* (8) (2020) 2178–2194.
[73] G. Chen, Electrochemical technologies in wastewater treatment, Sep. Purif. Technol. *38* (1) (2004) 11–41.
[74] W. Chen, X. Zhang, M. Mamadiev, Z. Wang, Sorption of perfluorooctane sulfonate and perfluorooctanoate on polyacrylonitrile fiber-derived activated carbon fibers: in comparison with activated carbon, RSC Adv. *7* (2) (2017) 927–938.
[75] R.K. Singh, S. Fernando, S.F. Baygi, N. Multari, S.M. Thagard, T.M. Holsen, Breakdown products from perfluorinated alkyl substances (PFAS) degradation in a plasma-based water treatment process, Environ. Sci. Technol. *53* (5) (2019) 2731–2738.
[76] M. Trojanowicz, A. Bojanowska-Czajka, I. Bartosiewicz, K. Kulisa, Advanced oxidation/reduction processes treatment for aqueous perfluorooctanoate (PFOA) and perfluorooctanesulfonate (PFOS)–A Review of Recent Advances, Chem. Eng. J. *336* (2018) 170–199.
[77] S. Yang, S. Fernando, T.M. Holsen, Y. Yang, Inhibition of perchlorate formation during the electrochemical oxidation of perfluoroalkyl acid in groundwater, Environ. Sci. Technol. Lett. *6* (12) (2019) 775–780.
[78] D. Wu, X. Li, J. Zhang, W. Chen, P. Lu, Y. Tang, L. Li, Efficient PFOA degradation by persulfate-assisted photocatalytic ozonation, Sep. Purif. Technol. *207* (2018) 255–261.
[79] G. Liu, H. Zhou, J. Teng, S. You, Electrochemical degradation of perfluorooctanoic acid by macro-porous titanium suboxide anode in the presence of sulfate, Chem. Eng. J. *371* (2019) 7–14.
[80] C. Zhang, T. Tang, D.R. Knappe, Oxidation of per-and polyfluoroalkyl ether acids and other per-and polyfluoroalkyl substances by sulfate and hydroxyl radicals: kinetic insights from experiments and models, Environ. Sci. Technol. (2023).
[81] C. Sandoval-Pauker, S. Yin, A. Castillo, N. Ocuane, D. Puerto-Diaz, D. Villagrán, Computational chemistry as applied in environmental research: opportunities and challenges, ACS EST Eng. *4* (1) (2024) 66–95, https://doi.org/10.1021/acsestengg.3c00227.
[82] Z. Chen, X. Wang, H. Feng, S. Chen, J. Niu, G. Di, D. Kujawski, J.C. Crittenden, Electrochemical advanced oxidation of perfluorooctanoic acid: mechanisms and process optimization with kinetic modeling, Environ. Sci. Technol. *56* (20) (2022) 14409–14417, https://doi.org/10.1021/acs.est.2c02906.
[83] N.E. Pica, J. Funkhouser, Y. Yin, Z. Zhang, D.M. Ceres, T. Tong, J. Blotevogel, Electrochemical oxidation of hexafluoropropylene oxide dimer acid (GenX): mechanistic insights and efficient treatment train with nanofiltration, Environ. Sci. Technol. *53* (21) (2019) 12602–12609, https://doi.org/10.1021/acs.est.9b03171.
[84] Y. Chen, M. Bhati, B.W. Walls, B. Wang, M.S. Wong, T.P. Senftle, Mechanistic insight into the photooxidation of perfluorocarboxylic acid over boron nitride, Environ. Sci. Technol. *56* (12) (2022) 8942–8952, https://doi.org/10.1021/acs.est.2c01637.